DOI: 10.13009/EUCASS2019-137



# Modelling and Control of Transition Flight of an eVTOL Tandem Tilt-Wing Aircraft

*Ludwik A. Sobiesiak*[⋆†], *Hugo Fortier-Topping*[‡], *David Beaudette*[⋆], *François Bolduc-Teasdale*[‡],
*Jean de Lafontaine*[⋆], *Amr Nagaty*[⋆], *David Neveu*[⋆], *David Rancourt*[‡]
[⋆]*NGC Aerospace Ltd.*
*2995 boul. Industriel, Sherbrooke, Quebec, J1L 2T9, Canada*
[‡]*Optis Engineering*
*4043 rue Brodeur, Sherbrooke, Quebec J1L 1K4, Canada*
ludwik.sobiesiak@ngcaerospace.com · hftopping@optisengineering.com
[†]Corresponding author

## Abstract

The EOPA aircraft is a tandem tilt-wing design capable of vertical take-off and landing. Essential to its operation is the ability to transition from powered-lift to fixed-wing flight, and vice-versa. Control of the transition maneuver is achieved by designing a nominal transition trajectory and using a gain-scheduled LQR to realize closed-loop control. Controller robustness to wind gusts is investigated. Methods used for the dynamic and aerodynamic modelling are described. Simulation results demonstrate the feasibility of closed-loop control of the transition maneuvers but also reveal a susceptibility to wind gusts encountered during transition.

## 1. Introduction

In the last few years, long-endurance vertical landing and take-off (VTOL) capable, fixed-wing UAV systems have firmly moved from the research to commercial domains. Piloted/human-carrying counterparts of such systems are not far behind. There is much interest in both electrically-powered aircraft for short-range "urban mobility" applications, which use only powered-lift to fly, and for longer-range electrically-powered VTOL (eVTOL) capable fixed-wing aircraft. The latter category of aircraft all share similar configuration characteristics: one or several primary fixed lifting surfaces for use during cruise flight and either some thrust vectoring capability or dedicated propulsion for powered-lift flight. Both the Vahana A3 and Mobi-One aircraft use a tilt-wing configuration to vector thrust in order to perform take-off/transition/landing operations; Eviation's Alice and Joby's S4 aircraft have tilt-rotor configurations for the same purpose; Terrafugia's TF-2 and Aurora Flight Science's PAV aircrafts have dedicated propulsion configurations, although in the case of the TF-2, the power system is a hybrid-electric solution.

This paper introduces the EOPA (Electrically-powered Optionally-Piloted) aircraft design, which finds itself in the same category as the A3 and Mobi-One aircraft, that is, a tilt-wing configuration. It is a configuration designed to be fully electric and to achieve the following performance requirements:

- a range of greater than 200 nautical miles (370 km);
- payload capacity of at least 600 lb (272 kg);
- recommended cruise speed of at least 100 kts at sea level (SL), international standard atmosphere (ISA).

The EOPA aircraft design is a tandem-wing configuration, with a primary front wing and secondary rear wing that is still large enough to provide a significant lift contribution. The design is the result of a multi-disciplinary design optimization process which sought to achieve the performance requirements set while balancing safety considerations, and ensuring the aircraft is completely electrically powered.

The aircraft has a distributed propulsion system, with eight variable RPM propellers distributed evenly along the forward wing and four propellers distributing along the rear wing. Propeller thrust axes are aligned with the chord line of the wing. There are no differences between the forward and rear propellers. Each wing is independently articulated and is capable of rotating from a position that is parallel with the fuselage of the aircraft (zeros degrees of rotation) to

DOI: 10.13009/EUCASS2019-137



a position that is perpendicular to the fuselage. The configuration has a total of nine control surfaces. Six ailerons are located on the forward wing, two elevators on the rear wing and a rudder on the tail.

The topic of this paper is the control strategy for the transition maneuver which takes the aircraft from powered-lift flight to wing-borne flight. The goal of the work presented herein is to demonstrate the initial feasibility of the design, assess whether transition is possible and qualify the robustness of transition to wind disturbances.

The remainder of paper is organised as follows: Section 2 describes the two key models used for simulating the aircraft: (1) the articulated multi-body dynamics model developed to simulate the tilt-wing action; (2) the aerodynamics model of the aircraft, which accounts for the induced flow over the wings from the aircraft propellers that is key to performing the transition maneuver. Section 3 describes the transition maneuver control strategy. The methodology for determining the transition trajectory is described, as is the gain-scheduled controller used to achieve closed-loop control. Simulated results for cruise-to-hover transitions are presented. Section 4 examines the robustness of the transition control strategy to discrete wind gusts.

## 2. Modelling

### 2.1 Articulated Dynamics Model

The EOPA aircraft is modelled as three separate bodies – fuselage, front wing, rear wing – held together by dynamical constraints. Such a model allows for the accurate determination of the torque and power required to actuate the wings during the different phases of flight and feeds back into the design process of the aircraft.

Figure 1 illustrates the key reference frames for the dynamics model. Frame $\mathcal{F}_i$ is the local Earth-fixed inertial frame; Frame $\mathcal{F}_0$ is the aircraft body frame, located at the aircraft fuselage's centre of mass; Frames $\mathcal{F}_k$, where $k = 1, 2$ correspond to the front and rear wings, respectively, are the wing body frames and rotate with the tilt angles of their respective wings. For the wing frame $k$, the 1-axis is parallel with the airfoil chord line, the 2-axis is parallel with the wing's axis of rotation in the direction of the right wing, and 3-axis completes the triad. The wing frame origins are located at their respective wing geometric centres, on their respective axis of rotation. The centres of mass of the wings lie along their respective frames' 1-axes, but are not coincident with their respective wing body frame origins. Let $\boldsymbol{\rho}_k$ (not illustrated) be the vector from the origin of $\mathcal{F}_k$ to the centre of mass of body $k$. Let the rotations between the inertial frame and the fuselage body frame be described by the rotation matrix $\mathbf{C}_{0i}$, and the rotations between the wing frames and the fuselage be described by the matrices $\mathbf{C}_{0k}$, for $k = 1, 2$.

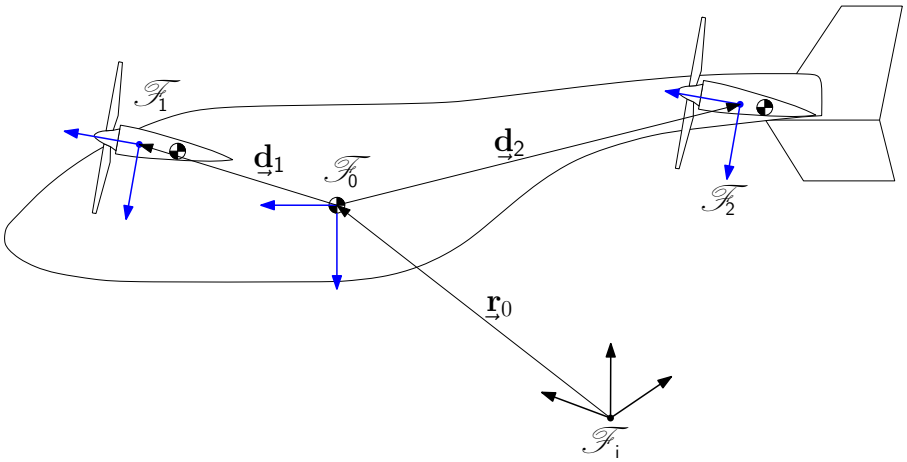


Figure 1: Articulated dynamics model reference frames.

The inertial position of the centre of mass of the fuselage is denoted by the vector $\mathbf{r}_0$. The inertial positions of the centres of mass of the two wings are given by

$$\mathbf{r}_k = \mathbf{r}_0 + \mathbf{C}_{i0}\mathbf{d}_k + \mathbf{C}_{i0}\mathbf{C}_{0k}\boldsymbol{\rho}_k. \tag{1}$$

Unless otherwise stated, vectors related to translation are all expressed in the inertial frame, while vectors related to attitude are expressed in the body frame of the body under consideration. Let $\gamma_k$by the angle between frames $\mathcal{F}_k$ and $\mathcal{F}_0$, measured about the 2-axis of $\mathcal{F}_k$.

DOI: 10.13009/EUCASS2019-137



Let $\mathbf{z}$ and $\boldsymbol{\nu}$ be the column matrices of the generalized coordinates and the generalized velocities of the system, respectively:

$$\begin{aligned}\mathbf{z} &= \begin{bmatrix} \mathbf{r}_0^\mathsf{T} & \mathbf{r}_1^\mathsf{T} & \mathbf{r}_2^\mathsf{T} & \mathbf{q}^{0i^\mathsf{T}} & \mathbf{q}^{1i^\mathsf{T}} & \mathbf{q}^{2i^\mathsf{T}} \end{bmatrix}^\mathsf{T} \\ \boldsymbol{\nu} &= \begin{bmatrix} \mathbf{v}_0^\mathsf{T} & \mathbf{v}_1^\mathsf{T} & \mathbf{v}_2^\mathsf{T} & \boldsymbol{\omega}_0^{0i^\mathsf{T}} & \boldsymbol{\omega}_1^{1i^\mathsf{T}} & \boldsymbol{\omega}_2^{2i^\mathsf{T}} \end{bmatrix}^\mathsf{T}\end{aligned} \tag{2}$$

where, for body $j = 0, 1, 2$, $\mathbf{r}_j$ is the body position expressed in the inertial frame, $\mathbf{v}_j$ is the body translational velocity expressed in the inertial frame, $\mathbf{q}^{ji}$ is the quaternion representing the body attitude relative to the inertial frame, and $\boldsymbol{\omega}_j^{ji}$ is angular velocity of the body with respective to the inertia frame, expressed in the body's body frame.

Differentiating $\boldsymbol{\nu}$ once and applying Newton's second law of motion, along with the appropriate constraint forces and torques, yields the equations of motions in the form of

$$\mathbf{M}\dot{\boldsymbol{\nu}} = \mathbf{f} - \boldsymbol{\nu}^\times \mathbf{H}\boldsymbol{\nu} + \mathbf{B}\mathbf{c}. \tag{3}$$

$\mathbf{M}$ is the system's mass matrix,

$$\mathbf{M} = \operatorname{diag}\left(\begin{bmatrix} m_0 & m_1 & m_2 & \mathbf{J}_0^0 & \mathbf{J}_1^1 & \mathbf{J}_2^2 \end{bmatrix}\right), \tag{4}$$

where the inertia matrices are all expressed in their respective body frames. The column matrix $\mathbf{f}$ is the matrix of external forces and torques acting on the different bodies

$$\mathbf{f} = \begin{bmatrix} \mathbf{f}_0^e \\ \mathbf{f}_1^e \\ \mathbf{f}_2^e \\ \mathbf{g}_0^e - \mathbf{g}_{01}^a - \mathbf{g}_{02}^a \\ \mathbf{g}_1^e + \mathbf{C}_{10}\mathbf{g}_{01}^a \\ \mathbf{g}_2^e + \mathbf{C}_{20}\mathbf{g}_{02}^a \end{bmatrix}, \tag{5}$$

with $\mathbf{f}_j^e$ and $\mathbf{g}_j^e$ being the external forces and torques, respectively, acting on body $j$, and $\mathbf{g}_{0j}^a = g_{0j}^a \hat{\mathbf{g}}_{0j}^a$ is the axial motor torque acting on body $j$.

The matrix $\boldsymbol{\nu}^\times$, allowing for a minor abuse of notation, is a block-diagonal matrix of skew-symmetric matrices

$$\boldsymbol{\nu}^\times = \operatorname{diag}\left(\begin{bmatrix} \mathbf{v}_0^\times & \mathbf{v}_1^\times & \mathbf{v}_2^\times & \boldsymbol{\omega}_0^{0i^\times} & \boldsymbol{\omega}_1^{1i^\times} & \boldsymbol{\omega}_2^{2i^\times} \end{bmatrix}\right), \tag{6}$$

and $\mathbf{H}$ is the inertia component of the system mass matrix

$$\mathbf{H} = \operatorname{diag}\left(\begin{bmatrix} 0 & 0 & 0 & \mathbf{J}_0^0 & \mathbf{J}_1^1 & \mathbf{J}_2^2 \end{bmatrix}\right). \tag{7}$$

The skew-symmetric operator is defined as

$$\mathbf{a}^\times = \begin{bmatrix} 0 & -a_3 & a_2 \\ a_3 & 0 & -a_1 \\ -a_2 & a_1 & 0 \end{bmatrix} \tag{8}$$

Lastly, the column matrix $\mathbf{c}$ contains the reaction forces and torques that dynamically constrain the three bodies together, and the matrix $\mathbf{B}$ kinematically defines how those forces and torques are applied. The joint linking a wing to the fuselage allows for no translation and rotation only about the wing frame's body 2-axis. Let the unit vectors $\hat{\mathbf{b}}_k$ and $\hat{\mathbf{c}}_k$ define the directions along which rotation motion is constrained, expressed in the fuselage body frame. The corresponding constraint torques can be written as $\mathbf{g}_k^b = g_k^b \hat{\mathbf{b}}_k$ and $\mathbf{g}_k^c = g_k^c \hat{\mathbf{c}}_k$, where $g_k^b$ and $g_k^c$ are scalar magnitudes. Therefore, $\mathbf{c}$ can be written as

$$\mathbf{c} = \begin{bmatrix} \mathbf{f}_{01}^{c^\mathsf{T}} & \mathbf{f}_{02}^{c^\mathsf{T}} & g_1^b & g_1^c & g_2^b & g_2^c \end{bmatrix}^\mathsf{T} \tag{9}$$

and

$$\mathbf{B} = \begin{bmatrix} -\mathbf{C}_{i0} & -\mathbf{C}_{i0} & \mathbf{0} & \mathbf{0} & \mathbf{0} & \mathbf{0} \\ \mathbf{C}_{i0} & \mathbf{0} & \mathbf{0} & \mathbf{0} & \mathbf{0} & \mathbf{0} \\ \mathbf{0} & \mathbf{C}_{i0} & \mathbf{0} & \mathbf{0} & \mathbf{0} & \mathbf{0} \\ -\mathbf{d}_{01}^\times & -\mathbf{d}_{02}^\times & -\hat{\mathbf{b}}_1 & -\hat{\mathbf{c}}_1 & -\hat{\mathbf{b}}_2 & -\hat{\mathbf{c}}_2 \\ \boldsymbol{\rho}_1^\times \mathbf{C}_{10} & \mathbf{0} & \mathbf{C}_{10}\hat{\mathbf{b}}_1 & \mathbf{C}_{10}\hat{\mathbf{c}}_1 & \mathbf{0} & \mathbf{0} \\ \mathbf{0} & \boldsymbol{\rho}_2^\times \mathbf{C}_{20} & \mathbf{0} & \mathbf{0} & \mathbf{C}_{20}\hat{\mathbf{b}}_2 & \mathbf{C}_{20}\hat{\mathbf{c}}_2 \end{bmatrix} \tag{10}$$

Due to the dynamical constraints of the system, the column matrix $\boldsymbol{\nu}$ contains generalized velocities that over-describe the system. The method of constraint elimination is applied to reduce the system of equations of motion, Eq. (3), to the

DOI: 10.13009/EUCASS2019-137



minimum number of equations required to describe the system. The minimum set of velocities needed to describe the system are:

$$\boldsymbol{\xi} = \begin{bmatrix} \mathbf{v}_0^\mathsf{T} & \boldsymbol{\omega}_0^{0i^\mathsf{T}} & \dot{\gamma}_1 & \dot{\gamma}_2 \end{bmatrix}^\mathsf{T}, \tag{11}$$

where $\dot{\gamma}_k$ are the angular rate of rotation of wing $k$ with respect to the fuselage. The states $\boldsymbol{\xi}$ and $\boldsymbol{\nu}$ are related by the constraint matrix $\mathbf{T}$, such that

$$\boldsymbol{\nu} = \mathbf{T}\xi, \tag{12}$$

where

$$\mathbf{T} = \begin{bmatrix} \mathbf{1} & \mathbf{0} & \mathbf{0} & \mathbf{0} \\ \mathbf{0} & \mathbf{1} & \mathbf{0} & \mathbf{0} \\ \mathbf{1} & -\mathbf{C}_{i0}\mathbf{d}_{01}^\times - \mathbf{C}_{i1}\boldsymbol{\rho}_1^\times\mathbf{C}_{10} & -\mathbf{C}_{10}\boldsymbol{\rho}_1^\times\mathbf{a}_1 & \mathbf{0} \\ \mathbf{1} & -\mathbf{C}_{i0}\mathbf{d}_{02}^\times - \mathbf{C}_{i2}\boldsymbol{\rho}_2^\times\mathbf{C}_{20} & \mathbf{0} & -\mathbf{C}_{20}\boldsymbol{\rho}_2^\times\mathbf{a}_2 \end{bmatrix} \tag{13}$$

and $\hat{\mathbf{a}}_k$ denotes the axis of rotation unit vector expressed in the wing $k$ body frame. Differentiating Eq. (12), substituting the result into the left hand side of Eq. (3) and solving for $\dot{\boldsymbol{\xi}}$ yields the following system of dynamical equations:

$$\dot{\boldsymbol{\xi}} = \left(\mathbf{T}^\mathsf{T}\mathbf{M}\mathbf{T}\right)^{-1}\left(\mathbf{T}^\mathsf{T}(\mathbf{f} - \boldsymbol{\nu}^\times\mathbf{H}\boldsymbol{\nu}) - \mathbf{T}^\mathsf{T}\mathbf{M}\dot{\mathbf{T}}\boldsymbol{\xi}\right). \tag{14}$$

Note, the term $\mathbf{T}^\mathsf{T}\mathbf{B}\mathbf{c}$ vanishes since the kinematic constraints $\mathbf{T}$ are orthogonal to the constraint forces $\mathbf{B}\mathbf{c}$. The values of $\dot{\mathbf{T}}$ are omitted for brevity. Eq. (14) is the form of the equations implemented in simulation.

Let the full state be

$$\mathbf{x} = \begin{bmatrix} \mathbf{r}_0^\mathsf{T} & \mathbf{q}^{0i^\mathsf{T}} & \gamma_1 & \gamma_2 & \mathbf{v}_0^\mathsf{T} & \boldsymbol{\omega}_0^{0i^\mathsf{T}} & \dot{\gamma}_1 & \dot{\gamma}_2 \end{bmatrix}^\mathsf{T}. \tag{15}$$

The aircraft position and wing tilt-angles are obtained by integrating their corresponding derivatives from the solution of $\boldsymbol{\xi}$. The aircraft attitude, represented by a quaternion, $\mathbf{q}^0i$, is obtained by integrating

$$\dot{\mathbf{q}}^{0i} = \begin{bmatrix} 0 & -\boldsymbol{\omega}_0^{0i^\mathsf{T}} \\ \boldsymbol{\omega}_0^{0i} & \boldsymbol{\omega}_0^{0i^\times} \end{bmatrix}\mathbf{q}^{0i}. \tag{16}$$

The external forces and torques acting on the different bodies warrant further examination. On the fuselage, the external forces are aerodynamic drag and gravity, while it is assumed the only external torque acting on it is the aerodynamic torque resulting from the offset between the fuselage's centre of mass and centre of pressure. On each wing, lift, drag and gravitational forces are present, as well as the propeller thrust forces; aerodynamic torques are also acting on each wing. The aerodynamics model describes how these forces are modelled.

### 2.2 Aerodynamics Model

The objective the aerodynamic model presented in this section is to capture the salient aerodynamic behavior of the aircraft as a function of vehicle states, control surface deflection, and propeller thrust, with limited computational cost. The approach uses a strip theory method,[2,9] for the lifting surfaces and empirical relationships for the fuselage aerodynamics based on experimental results from NASA on a rotorcraft fuselage.[17] This formulation is adapted to evaluate the external loads on aircraft for controller design. Special care is taken to consider propeller wash on the lifting surfaces, which is critical for tilt-wing VTOL transition.

In the strip theory approach, the wing is discretized into $n$ spanwise elements along each lifting surface. The aerodynamic properties of each wing section are evaluated using a table look-up method corrected for 3D effect using the relative local wind velocity containing contributions from the relative motion of the aircraft and the propeller-induced velocity.

Figure 2 illustrates several reference frames relative to the aerodynamics model: the front wing frame, $\mathcal{F}_{A_1}$, rear wing frame, $\mathcal{F}_{A_2}$, wing elements $\mathcal{E}_j$ frame, $\mathcal{F}_{\mathcal{E}_j}$ and the propeller frame $\mathcal{F}_{T_k}$, where $k = 1...8$ for the forward propellers, and $k = 9...12$ for the aft propellers. For wing element $\mathcal{E}_j$, the the air velocity expressed in $\mathcal{F}_{\mathcal{E}_j}$ due to the aircraft motion is

$$\mathbf{v}_j^\mathcal{E} = \mathbf{v}_0^{\mathcal{E}_j} + \left(\mathbf{C}_{\mathcal{E}_j0}\boldsymbol{\omega}_0^{0i}\right)^\times\mathbf{r}_j^\mathcal{E} - \mathbf{C}_{\mathcal{E}_ji}\mathbf{w}_j \tag{17}$$

where $\mathbf{v}_0^{\mathcal{E}_j}$ is the fuselage velocity as seen in $\mathcal{F}_{\mathcal{E}_j}$, $\mathbf{w}_j$ is the local wind seen by element $\mathcal{E}_j$ in the inertial frame, $\mathbf{C}_{\mathcal{E}_ji}$ and $\mathbf{C}_{\mathcal{E}_j0}$ are the rotation matrices describing the transformation to $\mathcal{F}_{\mathcal{E}_j}$ from $\mathcal{F}_\mathrm{i}$ and $\mathcal{F}_0$, respectively, and $\mathbf{r}_j^\mathcal{E}$ is the position vector of element $\mathcal{E}_j$, expressed in $\mathcal{F}_{\mathcal{E}_j}$. Eq. (17) is valid for slow wing rotation, which is a valid assumption for the proposed tilt wing configuration.

DOI: 10.13009/EUCASS2019-137



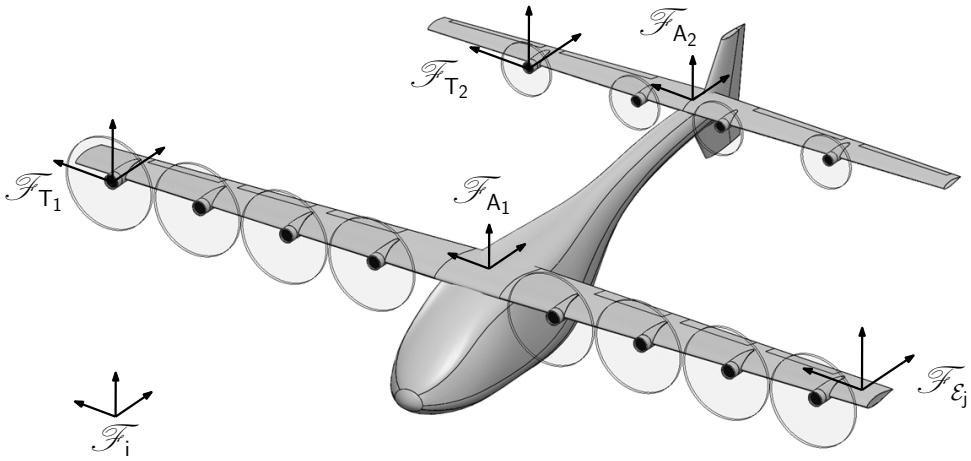


Figure 2: Aerodynamic model reference frames.

During transition or in hover, the thrust being generated by each propeller must be added to the velocity calculated by Eq. (17). An iterative process is used to find the local velocity seen by each wing elements by solving both for the contracted wake diameter, $D_c$, and increase in local velocity due to the thrusters.

First, the total velocity from the relative motion of element $\mathcal{E}_j$ and the local induced velocity by the propeller $k$ along $\hat{\mathcal{E}}_1^j$ axis, after contraction is

$$V_j = \left( \left( v_{j_1}^{\mathcal{E}} \right)^2 + \frac{2 f_k}{\rho S} \right)^{1/2} \tag{18}$$

where $f_k$ is the thrust generated by propeller $k = 1...12$, $S$ is the propeller disk area and $\rho$ is the air density, assuming complete contraction behind the propeller.[10]

The contracted wake diameter $D_c$ is given by

$$D_c = D \left( \frac{1+\mu}{2} \right)^{1/2}, \tag{19}$$

where $D$ is the propeller diameter and $\mu$, defined as

$$\mu = \frac{v_{j_1}^{\mathcal{E}}}{V_j} \tag{20}$$

is the ratio of the propeller wake speed to the local airspeed aligned with the wing chord at the element. Eq. (19) is used to assign which wing elements are included or excluded from the propeller wake based on the area covered by $D_c$. The normal velocity seen by each wing element remains unchanged by the presence of the propeller.

A mix of experimental data,[13,16] and analytical models[11] form the basis of the complete airfoil polars, for the lift, drag, and moments. Control surfraces are modeled through a shift in the lift curve slope of the airfoil section with an addition moment based on empirical data.[9,14] A reduction in the lift curve slope of the airfoil is considered due to the finite wing geometry. Fuselage loads are based on a rotorcraft experimental data[17] with a scale ratio of 0.78 based on geometric considerations. Rapid fuselage angular velocities are neglected in the modeling. Finally, the total aircraft external loads are obtained by summing the individual contributions of the elements of the lifting surfaces, the fuselage loads and the propeller forces.

## 3. Transition Flight Control Design

The control strategy for performing an autonomous maneuver consists of two components: a transition trajectory, which refers to a set of equilibrium points that spans the transition flight envelope from powered-lift flight to wing-borne flight; a closed-loop gain-scheduled controller that stabilizes the aircraft about each equilibrium point in the transition corridor.

The inputs available for control of the aircraft change depending on if the aircraft is in powered-lift or wing-borne flight. Table 1 summarizes the control inputs available in each configuration. Two additional control inputs are defined,

DOI: 10.13009/EUCASS2019-137



Table 1: Control Input Mapping for Powered-lift and Wing-borne Configurations

| State | Powered-Lift Control Input | Wing-Borne Control Input |
|---|---|---|
| Forward Speed | Pitch command | Propeller throttle |
| Lateral Speed | Roll command | n/a |
| Vertical Speed | Propeller throttle | Pitch command |
| Roll | Left/right differential thrust | Aileron deflection |
| Pitch | Forward/aft differential thrust | Elevator deflection |
| Yaw | Differential propeller torque | Rudder deflection |
| | Aileron deflection | Left/right differential thrust |

which are the wing hinge-motor torques, required to control the front and rear wing tilt-angles. Despite the aircraft's distributed propulsion, a simple, unified control vector, $\mathbf{u}$, can be defined:

$$\mathbf{u} = \begin{bmatrix} f_1 & \Delta f_1 & f_2 & \Delta f_2 & \delta_1 & \Delta\delta_1 & \delta_2 & \Delta\delta_2 & \delta_r & g^a_{01} & g^a_{02} \end{bmatrix}^{\mathsf{T}}, \tag{21}$$

where for the wing index $k = 1, 2$, $f_k$ is the collective propeller force, $\Delta f_k$ is the propeller thrust differential between left and right sides of the wing, $\delta_k$ is the collective control surface deflection, $\Delta\delta_k$ is the control surface deflection differential between left and right sides of the wing, $\delta_r$ is the rudder deflection, and $g^a_{0k}$ is the wing hinge control torque.

### 3.1 The Transition Trajectory

The transition trajectory is the reference trajectory the aircraft flies to transition from powered-lift flight to wing-borne flight, or vice-versa. It consists of a sequence of equilibrium or quasi-equilibrium points that correspond to specific wing-tilt angle and airspeed combinations. Such trajectories, sometimes referred to as transition corridors, are commonly used for performing transition maneuvers and mapping the transition flight envelope.[4,7,12]

An equilibrium point is an aircraft states vector and control input vector at which the net translational and angular accelerations acting on the aircraft are zero, i.e., given states, $\mathbf{x}^*$ and controls $\mathbf{u}^*$, $\dot{\boldsymbol{\xi}} = \boldsymbol{f}_{\xi}(\mathbf{x}^*, \mathbf{u}^*) = \mathbf{0}$; otherwise commonly known as a trim point. For quasi-equilibrium points, this constraint is relaxed for some states. The transition trajectory is therefore a set of trim points sequenced in terms of ascending or descending airspeed, to perform either hover-to-cruise or cruise-to-hover maneuver. Transition is achieved by exciting the controller with the reference signal of the next equilibrium point in the sequence, always driving it away from its equilibrium point.

Designing the transition trajectory using equilibrium points is possible but not necessarily desirable. By the nature of the transition maneuver, the aircraft will be at equilibrium prior to the start of the maneuver and upon its completion, but it will not be as it transitions between those two states. Thus, it does not necessarily make sense to design a trajectory linking the start and end equilibrium points with a sequence of intermediate equilibrium points.

Instead, the use of quasi-equilibrium points is proposed for the design of the transition trajectory. A quasi-equilibrium point is where non-zero accelerations on specific states are chosen to help in moving the aircraft to the next point in the transition trajectory sequence. The MATLAB function `trim` allows for the calculation of quasi-equilibrium points and has been used to calculate transition trajectories. This was accomplished by using the `trim` function to calculate the trim points of the full nonlinear dynamics model implemented in Simulink (articulated dynamic mode and aerodynamics model) for various airspeed/wing tilt-angle combinations and specifying the desired acceleration as an additional constraint.

An example transition trajectory to perform a cruise-to-hover transition maneuver is presented in Figures 3–5. Airspeed is the independent variable and the wing-tilt angles are the dependent variables. The transition trajectory has a total of 10 points and is designed for a descent rate of 2.5 m/s while transitioning to powered-lift flight. Figure 3 presents the wing-tilt angles, collective propeller thrusts and collective control surface deflections for the forward and rear wings, and the pitch of the aircraft, as they change with airspeed. Note, for the propeller thrusts, the point in the transition when the rear propellers engage is marked by a vertical dashed line. Figure 4 shows the required motor torques needed to actuate the wings during transition, and Figure 5 illustrates the vertical velocity profile of the trajectory along with the direction vectors of the "trimmed" acceleration of each trajectory point. The length of the arrows denotes the relative magnitude of the acceleration.

### 3.2 Gain-Scheduled LQR Control

A number of approaches have been proposed for performing closed-loop control of a transition maneuver, including simple PD control with feed-forward trim controls;[8] design of a nonlinear Lyapunov controller;[3] and gain-scheduled

DOI: 10.13009/EUCASS2019-137



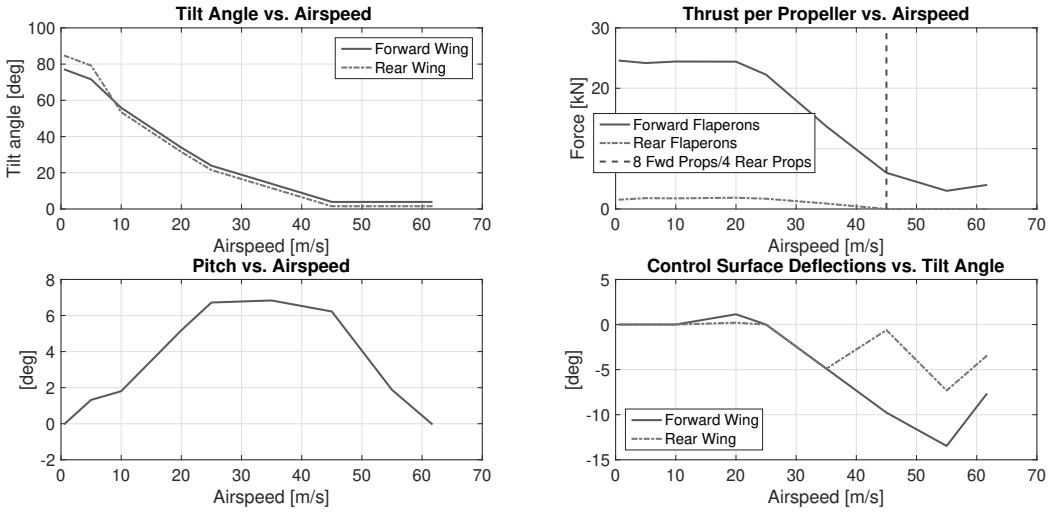


Figure 3: Trim control inputs and pitch versus airspeed for a cruise-to-hover transition trajectory.

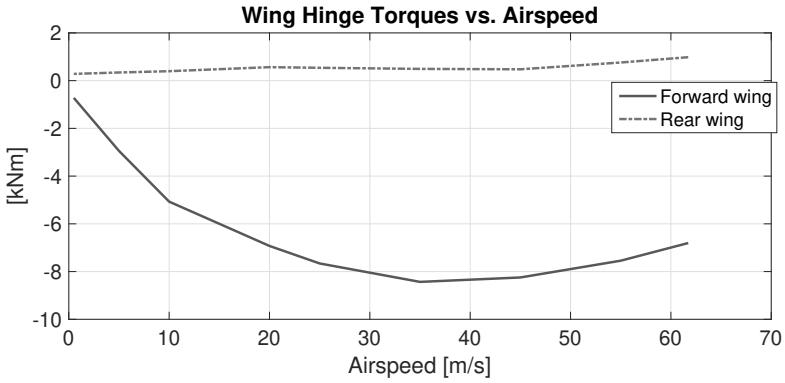


Figure 4: Wing hinge control torques versus airspeed for a cruise-to-hover transition trajectory.

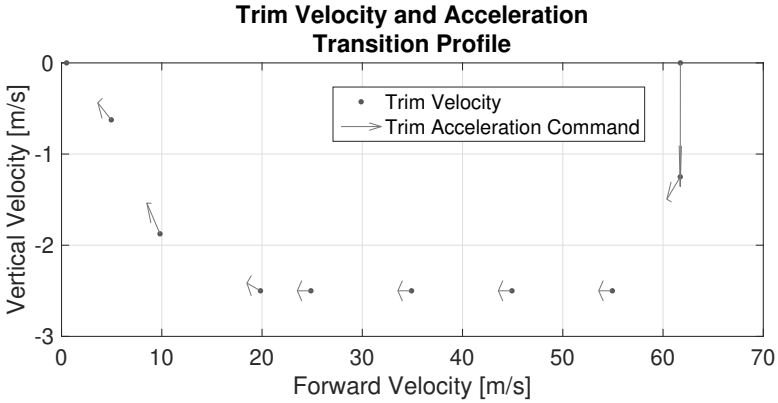


Figure 5: Vertical versus forward velocity profile for a cruise-to-hover transition trajectory. Arrows denote trim acceleration directions and relative magnitudes at each point in the trajectory.

H-infinity control.[6] In this paper, a gain-scheduled linear quadratic control architecture is proposed.

Let $\mathcal{X}_k = \{\mathbf{x}_k^*, \mathbf{u}_k^*\}$ for $k = 1...N$, be set of trim points defining the transition trajectory and $V_k$ be the nominal airspeed associated with the $k^{th}$ trim point.

DOI: 10.13009/EUCASS2019-137



Given the current airspeed of the aircraft, $V(t)$, the gain-scheduling variable $\sigma(t)$ is defined as

$$\sigma(t) = \frac{V(t) - V_k}{V_{k+1} - V_k}, \qquad V_{k_1} > V(t) > V_k, \tag{22}$$

The control input vector is scheduled according to

$$\mathbf{u}(t) = \begin{cases} \mathbf{u}_1(t), & V(t) \leq V_1 \\ (1 - \sigma(t))\mathbf{u}_k(t) + \sigma(t)\mathbf{u}_{k+1}(t), & V_{k+1} > V(t) > V_k \\ \mathbf{u}_N(t), & V(t) \geq V_k \end{cases} \tag{23}$$

The control input signal, $\mathbf{u}_k(t)$, is given by

$$\mathbf{u}_k(t) = \mathbf{u}_k^*(t) + \Delta\mathbf{u}_k(t), \tag{24}$$

where $\mathbf{u}_k^*(t)$ is the trim control vector corresponding to $\mathcal{X}_k$, and $\Delta\mathbf{u}_k(t)$ is feedback control vector from the linear-quadratic regulator (LQR) designed for the linearized dynamical system associated with $\mathcal{X}_k$.

Linearizing the nonlinear dynamics of the system (Eq. (14) – (16)) about each point in the transition trajectory, $\mathcal{X}_k$, yields a set of $N$ linear systems of the form

$$\dot{\mathbf{e}}(t) = \mathbf{A}_k\mathbf{e}(t) + \mathbf{B}_k\Delta\mathbf{u}_k(t), \tag{25}$$

where $\mathbf{e}(t) = \mathbf{x}(t) - \mathbf{x}_k^*$. Note, the lateral aircraft positions are cyclic coordinates and have no impact on the transition dynamics. Consequently, they are not under closed-loop control during transition.

An optimal feedback gain for each linear system is calculated per

$$\Delta\mathbf{u}_k = -\mathbf{K}_k\mathbf{e}(t) = -\mathbf{R}_k^{-1}\mathbf{B}_k^\mathsf{T}\mathbf{P}_k\mathbf{e}(t), \tag{26}$$

where $\mathbf{P}_k$ is the solution to the steady-state Riccati equation

$$\mathbf{0} = \mathbf{A}_k\mathbf{P}_k + \mathbf{P}_k\mathbf{A}_k^\mathsf{T} - \mathbf{P}_k\mathbf{B}_k\mathbf{R}_k^{-1}\mathbf{B}_k^\mathsf{T}\mathbf{P}_k + \mathbf{Q}_k, \tag{27}$$

and $\mathbf{Q}_k$ and $\mathbf{R}_k$ are quadratic penalty matrices on the state error and control inputs, respectively.

The control input penalty matrices $\mathbf{R}_k$, $k = 1...N$, must be judiciously chosen for their particular trajectory points. For trajectory points at high airspeeds and low wing tilt-angles, $\mathbf{R}_k$ must heavily penalize the use the propeller force control inputs and favor the use of control surface deflections. For trajectory points at low airspeeds and large wing tilt-angles, the penalization strategy is reversed, so that propellers forces are favored over control deflections.

### 3.3 Simulation Results

The models described in Section 2 and the control strategy described in Section 3 have been implemented in a MATLAB/Simulink simulation. The simulation includes realistic approximations of control surface and propeller response dynamics. Results will be limited to the maneuver transitioning the aircraft from a cruise state to a powered-lift, i.e., hover state. Hover-to-cruise transition has also been successfully demonstrated during this project, but is considered the "easier" of the transition maneuvers: decelerating and stopping the aircraft is more challenging than accelerating it; consequently, this paper focuses on the cruise-to-hover transition results.

Simulation results showing a nominal cruise flight to hover transition maneuver, realized by the proposed control strategy are presented in Figures 6–8. The initial conditions of the aircraft are that of it being in a level-flight, cruise configuration: it is traveling at an airspeed of 61.7 m/s (120 knots), at an altitude of 305 m (1000 feet). The goal is to bring the aircraft to rest, in a powered-lift configuration. The duration of the maneuver is approximately 55 s. The transition trajectory used for the simulation is the one described in the figures in Section 3.1. As shown in Figure 5, the transition trajectory is designed to maintain a constant descent velocity of 2.5 m/s (~500 feet/min) during the majority of the maneuver. Figure 6 shows that both the forward and vertical velocities of the transition trajectory are tracked well. Pitch control performance is not ideal. Large deviation from the command is observed at approximate 30 s and over all, it is a bumpy ride for a hypothetical passenger. Further refinement of the trajectory design and controller tuning is needed.

Figure 7 presents the control inputs required to perform the transition maneuver, while Figure 8 illustrates the wing hinge torques required to articulate the wings.

DOI: 10.13009/EUCASS2019-137



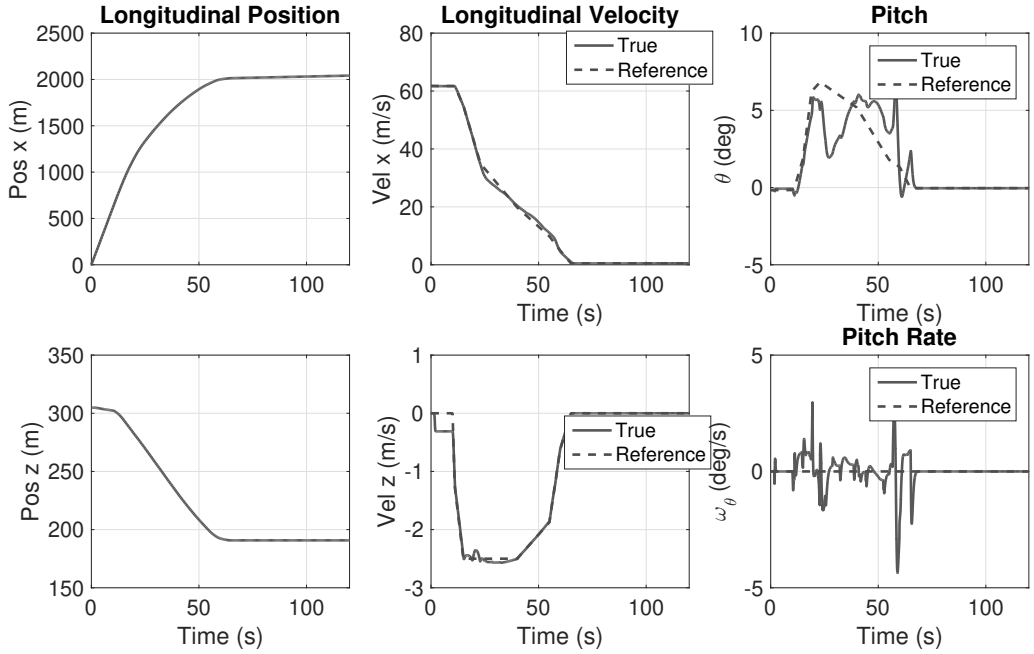


Figure 6: Longitudinal states during a cruise-to-hover transition maneuver, no wind conditions.

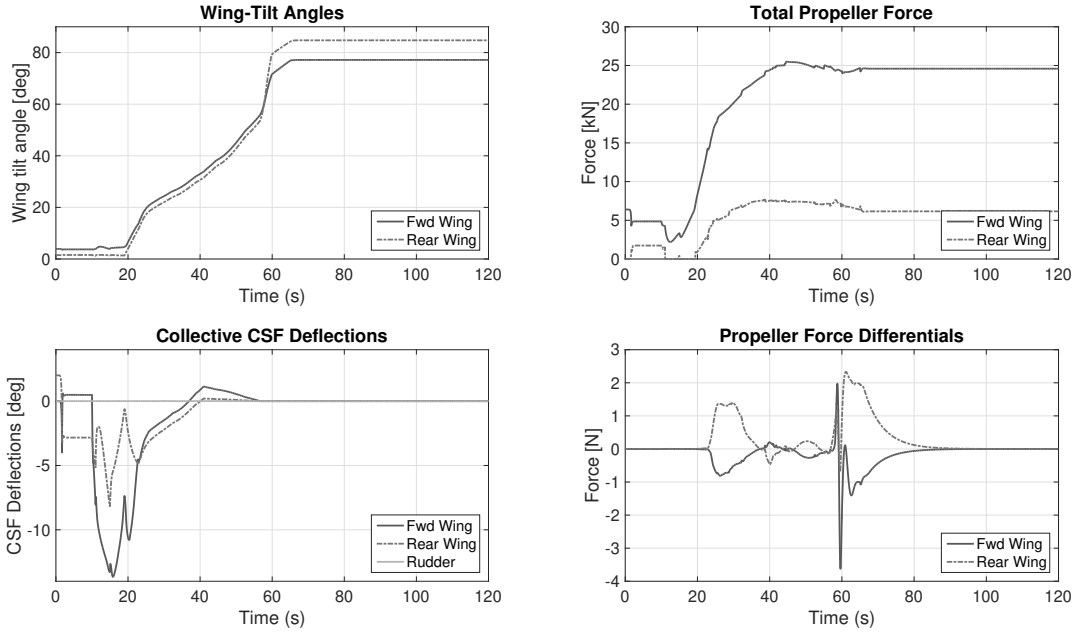


Figure 7: Wing tilt angles and control inputs for a cruise-to-hover transition maneuver, no wind conditions.

## 4. Gust Sensitivity Analysis

This section investigates the robustness of the transition controller when the EOPA aircraft encounters a discrete gust while transitioning from cruise flight to powered-lift flight. This investigation is motivated by a concern that a wind gust could stall a large section of the aircraft's wing during transition, resulting in a large lateral perturbation, and destabilize the aircraft in an unrecoverable fashion.

DOI: 10.13009/EUCASS2019-137



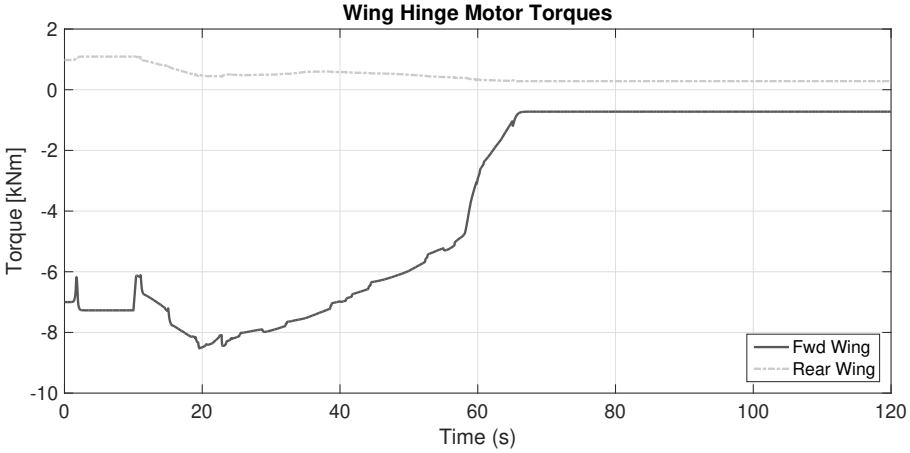


Figure 8: Applied wing hinge torques during a cruise-to-hover transition maneuver, no wind conditions.

### 4.1 Discrete Gust Model

The discrete gust model, as described by the Federal Aviation Administration,[1] is used. The gust velocity is modelled by

$$W_g = \frac{W_m}{2}\left(1 - \cos\left(\frac{\pi x}{d_m}\right)\right), \quad 0 < x < 2d_m, \tag{28}$$

where $W_m$ is the maximum gust magnitude, $d_m$ is the difference in radius of the inner and outer regions of influence and $x$ is the distance penetrated into the gust.

The gust model consists of two concentric spheres of influence: in the inner sphere, the wind speed is at a maximum; between the two spheres, the wind speed increases with decreasing distance to the centre, as describes per Eq. (28); outside the outer sphere, wind gust velocity is zero.

To assess the EOPA aircraft's sensitivity to wind gusts, a very specific test case was developed in which the aircraft encounters a wind gust that affects only half of the aircraft and results in a stall of only half of the two wings. Figure 9 illustrates this wind gust scenario that results in an asymmetric stall. This analysis has considered a single

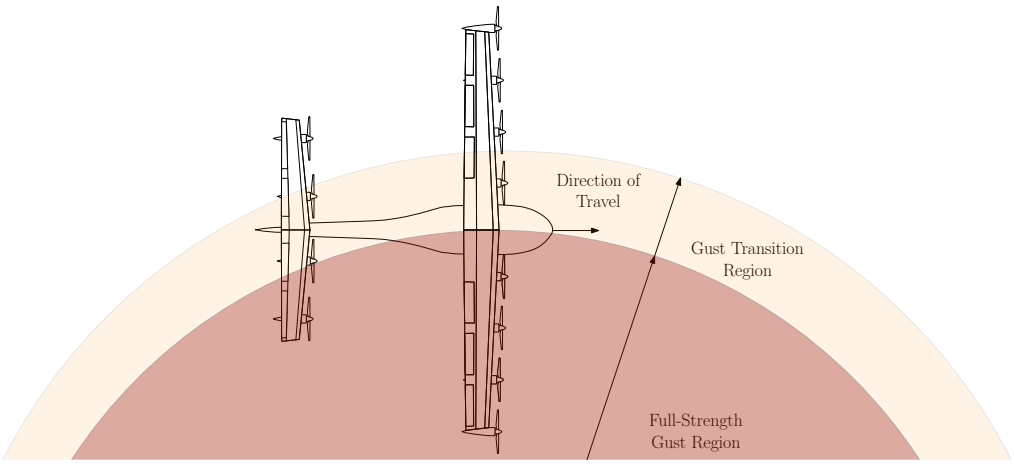


Figure 9: Discrete gust encounter resulting in an asymmetric stall.

gust direction for all gust magnitude cases and application times. The gust direction unit vector for all cases, expressed in the aircraft's heading frame, is $\hat{\mathbf{w}} = [\frac{1}{\sqrt{2}} \;\; 0 \;\; \frac{1}{\sqrt{2}}]^\mathsf{T}$, which corresponds to a gust blowing up and into the aircraft, with an incidence of 45 degrees. There is no lateral component to the gust. This direction has the effect of dramatically increasing the angle of attack on the portion of the wing that encounters the gust.

Recall Eq. (17), which describes the airspeed of an individual element of the wing. As a portion of the aircraft passes through the gust, different elements along the wing will penetrate a different amount into the gust and thus

DOI: 10.13009/EUCASS2019-137



experience different magnitudes of wind. This results in some sections of the wing possibly experiencing a stall, while other sections remain unstalled.

### 4.2 Feed-Forward Gust Rejection

A preliminary set of simulations that tested the transition controller in the presence of wind revealed a high sensitivity to wind gusts. The aircraft could be destabilized by small gusts encountered at any time during the transition maneuver. This prompted an investigation into possible gust mitigation/rejection strategies.

For the following gust rejection strategy, a means of gust detection is required. The following gust estimation strategy is proposed: the aircraft has 3D-airspeed sensors located at each wing tip, as well as on the fuselage; using the aircraft's attitude and attitude rate knowledge, the approximate magnitude and direction of a wind gust hitting one section of a wing can be estimated to within a reasonable accuracy. Refs. 5, 15 suggest that such a gust detection scheme is feasible.

The feed-forward control strategy itself is rudimentary. Let the linearized dynamics of the system be given by

$$\dot{\mathbf{e}} = \mathbf{A}_k\mathbf{e} + \mathbf{B}_k\mathbf{u} + \mathbf{G}_k\mathbf{w}, \tag{29}$$

where $\mathbf{u}$ is the control vector, $\mathbf{w} = [\mathbf{w}_{1r}^\mathsf{T} \;\; \mathbf{w}_{1l}^\mathsf{T} \;\; \mathbf{w}_{2r}^\mathsf{T} \;\; \mathbf{w}_{2l}^\mathsf{T}]^\mathsf{T}$ is the $12 \times 1$ vector of wind gusts seen on the forward right, forward left, rear right and rear left wings and $\mathbf{G}_k$ is the input vector that relates how the half-wing wind gust vectors affect the error dynamics. This assumes that all the elements of a half-wing of the aircraft experience the same wind gust magnitude. Under this assumption, in order to perfectly compensate for the wind gust, the feed-forward control must be

$$\mathbf{u}_{ff} = -\left(\mathbf{B}_k^\mathsf{T}\mathbf{B}_k\right)^{-1}\mathbf{B}_k^\mathsf{T}\mathbf{G}_k\mathbf{w}, \tag{30}$$

assuming the inverse $\left(\mathbf{B}_k^\mathsf{T}\mathbf{B}_k\right)^{-1}$ exists. It is recognized that due to sensing errors and delays, and actuation delays, perfect feed-forward control is impossible. Nevertheless, even with such delays, simulations show the proposed feed-forward strategy can significantly reduce the impact of gusts. In the context of the EOPA configuration, it is undesirable to calculate feed-forward components for all the control signals; rather, a subset of control signals consisting of differential thrusts between left and right propellers on the forward and rear wings, wing-hinge control torques, forward wind aileron and rudder deflections are used. The corresponding $\left(\mathbf{B}_k^\mathsf{T}\mathbf{B}_k\right)^{-1}$ for this control signal subset remains invertible throughout the transition trajectory, so the feed-forward control vector remains computable. The matrix $\left(\mathbf{B}_k^\mathsf{T}\mathbf{B}_k\right)^{-1}\mathbf{B}_k^\mathsf{T}\mathbf{G}_k$ is calculated for the different transition trajectory trim points and gain-scheduled with airspeed, so that the matrix is always appropriate for the flight conditions during transition. This feed-forward strategy is used in the gust rejection test cases to improve stability in the presence of gusts.

In addition to this feed-forward strategy, upon the detection of a gust, the transition maneuver is "paused" to allow the aircraft to stabilize itself before continuing with the transition maneuver. This means that the reference signal driving the transition maneuver holds the last point in the transition trajectory when the gust is detected, rather than commanding the subsequent point trajectory. This prevents unnecessary excitation of the aircraft while it is recovering from a gust perturbation.

### 4.3 Cruise-to-Hover Transition in the Presence of a Gust

To study the transition controller's sensitivity to a discrete gust, a simulation campaign was performed, where the aircraft, while performing a cruise-to-hover transition maneuver, encounters a discrete gust. The timing of when the aircraft encounters the gust, and the magnitude of the gust were both varied. For near-cruise conditions (wing tilt angles less than 10 degrees, airspeed greater than 55 m/s) and near-hover conditions (wing tilt angles greater than 70 degrees, airspeed near 0 m/s), the transition controller, using the gust rejection strategy, could recover from perturbations caused by a gust of up to 13 m/s (25 knots). For intermediate points in the transition trajectory, the aircraft was much more sensitive to perturbations caused to a discrete gust. For wing tilt angles between 20 - 60 degrees, a wind gust between 3 - 6 m/s (6 - 12 knots) could destabilize the aircraft, despite the gust rejection strategy.

A numerical example illustrates the successful rejection of a gust during transition. The initial conditions are identical to the nominal case described in Section 3.3. During this test case, a discrete gust, as described previously, is encountered 48 seconds into the simulation, when the aircraft is approximately a quarter of the way through the transition maneuver. Forward and rear tilt angles are at 19 and 27 degrees, respectively. Figure 10 shows the immediate impact of the gust, stalling a quarter of the right front wing. The impact of this asymmetric stall is seen in Figure 11, where the resulting large roll and yaw perturbations are evident at the 48 s. Figures 12 and 13 show that the lateral perturbations are corrected for using a combination of differential thrust control, rudder and aileron control. It is

DOI: 10.13009/EUCASS2019-137



observed that this 5 m/s gust is already near the limit of what the aircraft can reject: rudder control and forward propeller differential thrust control signals all saturate during the gust rejection and recovery. Indeed, the aircraft is unable to recover from the perturbation for the same scenario but with a gust magnitude of 6 m/s.

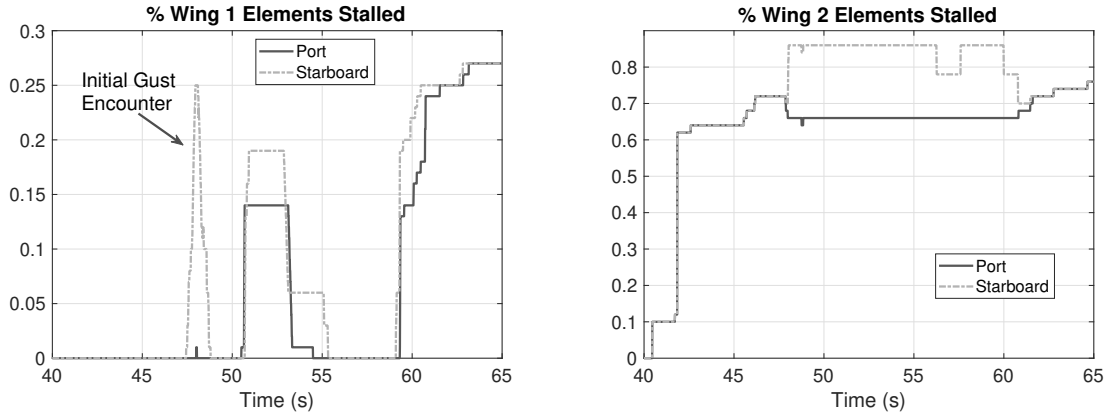


Figure 10: Percentage of stalled wing elements during transition when encountering a wind gust.

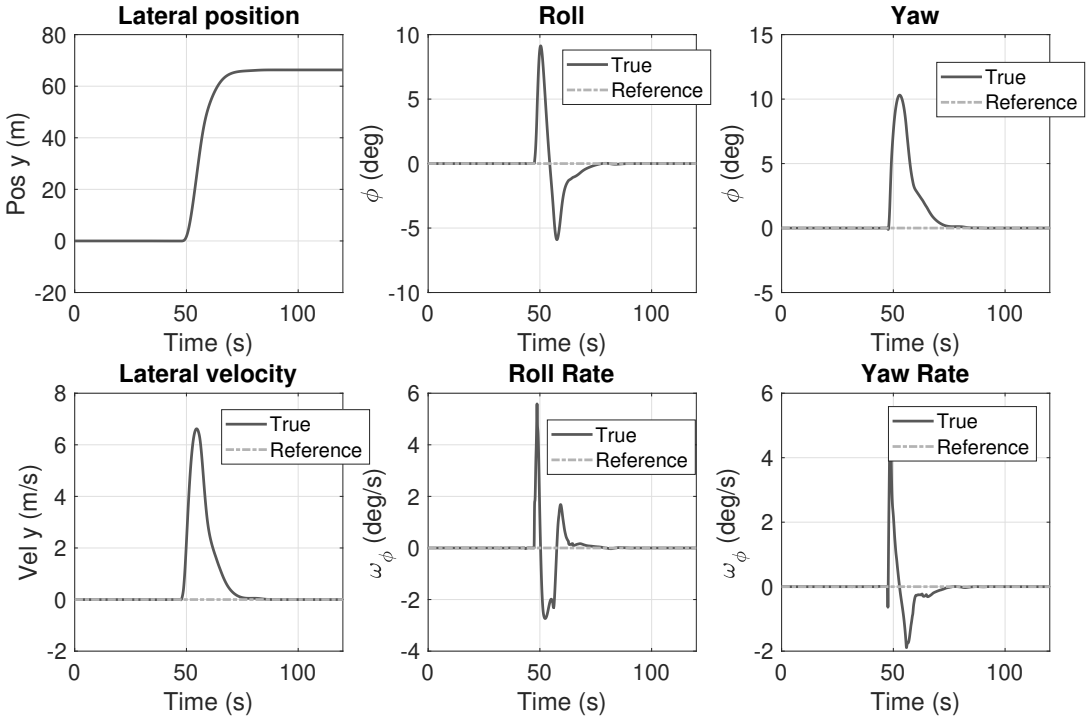


Figure 11: Lateral state perturbations due to discrete wind gust during transition.

## 5. Conclusions

The proposed closed-loop transition control strategy demonstrates that autonomous control of the EOPA aircraft during a transition maneuver is feasible. Although only cruise-to-hover transition results have been presented in this paper, successful transition maneuvers in both directions have been simulated as a part of this project. The aircraft configuration is sensitive to wind gusts, which can result in a potentially destabilizing roll/yaw perturbation, particularly when such a gust is encountered while performing a transition maneuver. Although the proposed feed-forward gust rejection

DOI: 10.13009/EUCASS2019-137



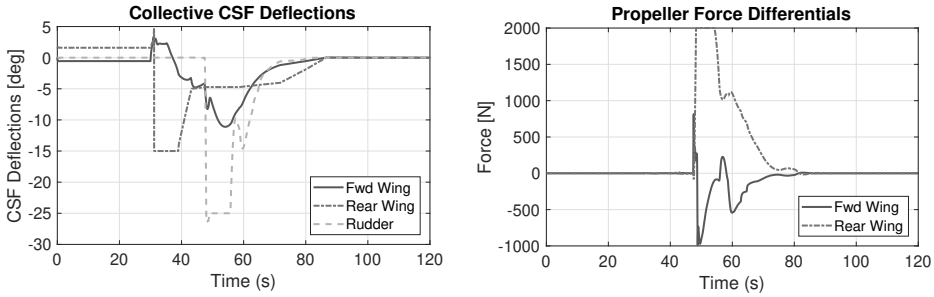


Figure 12: Collective control surface deflections and propeller force differentials for gust rejection during transition.

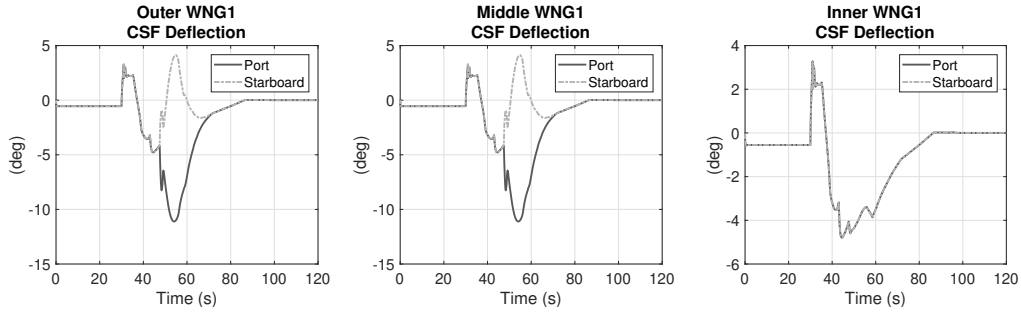


Figure 13: Wing 1 control flaperon deflections for gust rejection during transition.

strategy does help in rejecting the gust perturbation in some cases, in general if a gust of moderate intensity is encountered during the transition maneuver, the vehicle appears to lack the control authority to reject the perturbation, at least for the current control architecture.

There are several avenues for future work. Although closed-loop control was successfully demonstrated with the current architecture, tuning of the system was not straightforward and it is believed that a simpler transition architecture can be achieved by decoupling the control allocation to the actuators from the transition trajectory tracking. This separation will allow for a potentially non-gain-scheduled transition controller to communicate force and torque commands to a control allocation function, that then determines the commands for the appropriate actuators for the current flight conditions. Regarding the gust rejection, further investigation into gust rejection techniques is required. Investigation into the configuration of the aircraft itself, in particular its vertical stabilizer, is also needed in order to fully explore the options available to make the aircraft more robust to wind gusts.

## 6. Acknowledgments

This work was done as part of the EOPA Conceptual Design Program, under the leadership of Zenith Altitude. Funding for the program was provided was provided by Lung Biotechnology PBC.

## References

[1] Dynamic gust loads. Advisory Circular AC 25.341-1, Federal Aviation Administration, 2014.

[2] M. Bronz and A. Drouin. Preliminary Design Estimation of the V/STOL Airplane Performance. *International Journal of Micro Air Vehicles*, 7(4):449 – 462, December 2015.

[3] J. J. Dickeson, D. Miles, O. Cifdaloz, V. L. Wells, and A. A. Rodriguez. Robust LPV H-Infinity Gain-Scheduled Hover-to-Cruise Conversion for a Tilt-Wing Rotorcraft in the Presence of CG Variations. In *2007 American Control Conference*, pages 5266–5271, July 2007.

[4] G. Droandi, M. Syal, and G. Bower. Tiltwing Multi-Rotor Aerodynamic Modeling in Hover, Transition and Cruise Flight Condition. In *AHS International 74th Annual Forum & Technology Display*, 2018.

[5] B. Etkin and L.D. Reid. *Dynamics of Flight: Stability and Control, Third Edition*. John Wiley & Sons, Hoboken, NJ, 1996.

DOI: 10.13009/EUCASS2019-137



[6] G. Flores and R. Lozano. Transition flight control of the quad-tilting rotor convertible mav. In *2013 International Conference on Unmanned Aircraft Systems (ICUAS)*, pages 789–794, May 2013.

[7] William J. Fredericks, Robert G. McSwain, Brian F. Beaton, and David W. Klassman. Greased Lightning (GL-10) Flight Testing Campaign. Technical Memorandum NASA/TM-2017-219643, NASA, July 2017.

[8] P. Hartmann, C. Meyer, and D. Moormann. Unified Velocity Control and Flight State Transition of Unmanned Tilt-Wing Aircraft. *J. Guidance, Dynamics and Control*, 40:1348 – 1359, June 2017.

[9] A. Jameson. The analysis of propeller-wing flow interaction. Analytic Methods in Aircraft Aerodynamics. In *NASA Symposium Proceedings SP-228*, pages 721–749, October 1969.

[10] W. Johnson. *Rotorcraft Aeromechanics*. Cambridge University Press, Cambridge, 2013.

[11] F. Mahmuddin, S. Klara, H. Sitepu, and S. Hariyanto. Airfoil Lift and Drag Extrapolation with Viterna and Montgomerie Methods. *Energy Procedia*, 105:811 – 816, May 2017.

[12] Koji Muraoka, Noriaki Okada, Daisuke Kubo, and Masayuki Sato. Transition Flight of a Quad-Tilt Wing VTOL UAV. In *28th International Congress of the Aeronautical Sciences*, 2012.

[13] C. Ostowari and D. Naik. Post-stall wind tunnel data for naca 44xx series airfoil sections. Technical Report SERI/STR-217-2559, 5791328, U.S. Department of Energy, January 1982.

[14] D. Raymer. *Aircraft Design: A Conceptual Approach, Fifth Edition*. American Institute of Aeronautics and Astronautics, Inc., Washington, DC, 2012.

[15] C.D. Regan and C.V. Jutte. Survey of Applications of Active Technology for Gust Alleviation and New Challenges for Lighter-weight Aircraft. Technical Memorandum NASA/TM-2012-216008, NASA, April 2012.

[16] R. E. Sheldahl and R. C. Klimas. Aerodynamic characteristics of seven symmetrical airfoil sections through 180-degree angle of attack for use in aerodynamic analysis of vertical axis wind turbines. Technical Report SAND-80-2114, Sandia National Labs, March 1981.

[17] P .Talbot, B. Tinling, W. Decker, and R. Chen. A mathematical model of a single main rotor helicopter for piloted simulation. NASA Technical Memorandum 84281, NASA, September 1982.